J Nanopart Res (2014) 16:2529
DOI 10.1007/s11051-014-2529-5

RESEARCH PAPER

Surface, thermal, and mechanical properties of composites and nanocomposites of polyurethane/PTFE nanoparticles

P. S. Anbinder · P. J. Peruzzo · A. de Siervo · J. I. Amalvy

Received: 6 August 2013 / Accepted: 18 June 2014 / Published online: 3 July 2014

Abstract Films from blends of polyurethane and nano-polytetrafluoroethylene aqueous dispersions (PU/nanoPTFE) were prepared, and the effect of the addition of different amounts of PTFE nanoparticles (50 nm) was studied. The changes in the superficial properties of the films were studied by means of XPS, ATR/FTIR, and contact angle measurements. SEM and TEM results are also included. The contact angle values confirm the surface hydrophobicity of composite films. Even though nanoparticles are present in the bulk, higher concentrations of particles appear at the surface in samples with lower nanoPTFE content (up to 10 wt%), as revealed by XPS. Higher amounts of nanoPTFE particles cause aggregation. The mechanical and thermal properties of composites are also discussed.

Keywords Polyurethane · PTFE nanoparticles · Composite materials · Low-energy surface · Contact angle · XPS

P. S. Anbinder · P. J. Peruzzo · J. I. Amalvy
Grupo (Nano)Materiales Poliméricos, Instituto de Investigaciones Fisicoquímicas Teóricas y Aplicadas (INIFTA), (CCT La Plata - CONICET- Universidad Nacional de La Plata), Diag. 113 y 64, La Plata, Argentina

A. de Siervo
Departamento de Física Aplicada, Instituto de Física "Gleb Wataghin", Universidade Estadual de Campinas, UNICAMP, Campinas, Brazil

J. I. Amalvy (✉)
Centro de Investigación y Desarrollo en Tecnología de Pinturas(CIDEPINT), Av. 52 entre 121 y 122; Centro de Investigación y Desarrollo en Ciencia y Tecnología de Materiales (CITEMA), Facultad Regional La Plata (Universidad Tecnológica Nacional), 60 y 124 y Cátedra Materiales Poliméricos, Facultad de Ingeniería, Universidad Nacional de La Plata, Calle 1 y 47, La Plata, Argentina
e-mail: jamalvy@inifta.unlp.edu.ar; jamalvy@gmail.com

Introduction

Various methods have been reported for the preparation of hydrophobic surfaces, like electrochemical reaction and deposition (Meng et al. 2008; Li et al. 2003), chemical vapor deposition (Zheng et al. 2009), etching method (Pan et al. 2009), surface modification (Jeong et al. 2006), electro-spinning, and lithography (Zhu et al. 2006; Lai et al. 2008) or sol–gel techniques (Lakshmi and Basu 2009). These methods create a rough micro/nanostructure on a hydrophobic substrate surface or modify them with low surface energy materials such as fluorinated or silicon compounds. However, these methods generally present some disadvantages, for instance cost and unpractical application. Yamauchi et al. (2005) reported the incorporation of PTFE nanoparticles to prepare a water-repellent coating for mobile phone microphones. High water repellency was attributed to both the surface roughness formed by the PTFE particles on

the surface of the coating and the existence of air under the water droplets on the surface of the coating. As the concentration of PTFE increases, higher contact angles are obtained. More recently, Huang et al. (2011) have incorporated PTFE nanoparticles in polyoxymethylene to modify the tribological properties.

On the other hand, polyurethanes (PU) are perhaps the most versatile polymers material used in coatings with a wide variety of physical and chemical properties, derived from the possibility of tailoring these properties from many commercially available and relatively inexpensive polyols, isocyanates, and chain extenders. Water-based polyurethane dispersions (PUDs) have received increased attentions because they are non-toxic, non-flammable, and do not pollute the environment like solvent-based materials. Systems based on PUDs show excellent film properties and possess a high outdoors resistance, to grazing and UV radiation. However, the hydrophilic segments of PU adversely affect the water and oil repellency of films due to the relatively high surface free energy (Król 2007).

The incorporation of fluorine atoms into the polymer chain would give the PU films special surface properties since these species are expected to migrate to the surface, resulting in a considerable decrease in the surface energy. The incorporation of fluorine into polyurethane matrixes introduces changes in the final properties such as chemical, thermal, hydrolytic, and oxidative stability. In order to obtain a material with good surface properties, fluorinated modifiers need to be concentrated at the film/air interface (Lee et al. 2007). This goal could be achieved by taking advantage of the tendency of surface segregation of fluorinated species.

Recently, Liu et al. (2011) have reported the preparation of PU/PTFE composites for preparing superhydrophobic coatings using a solvent-based procedure. They found that an irregular rough structure with dispersed grooves and protuberances was responsible for the surface superhydrophobicity.

However, to our best knowledge, there are no reports about preparing hydrophobic water-based coatings using composites from aqueous polyurethane and nanoPTFE dispersions. In this work, surface-modified PTFE nanoparticles (nanoPTFE) were blended with a PU dispersion to obtain PU/nanoPTFE composites. Surfaces were subsequently examined by static contact angle measurements and by X-ray photoelectron spectroscopy (XPS). In addition, interaction between the nanoparticles and the polyurethane chains was studied by FTIR spectroscopy. With low nanoPTFE content (up to 10 wt%), a self-stratifying dispersion is obtained after drying.

Experimental

Materials

Isophorone diisocyanate (IPDI, Aldrich), 2-hydroxy ethylmethacrylate (HEMA, Aldrich), potassium persulfate (KPS, Anedra), hydrazine monohydrate (HZN, Aldrich), triethylamine (TEA, U.V.E.), and dibutylindilaurate (DBTDL, Aldrich) were of analytical grade and were used as received. Polypropylene glycol 1000 (PPG1000, Voranol 2110) was dried and degassed at 80 °C at 1–2 mm Hg before use. Dimethylol propionic acid (DMPA, Aldrich) was dried at 100 °C for 2 h in an oven. TEA was also dried before use.

The nanoPTFE aqueous dispersion (Algoflon® MD10 PTFE, nominal average particle size ca. 50 nm, $\zeta = -51$ mV) was donated by Solvay Specialty Polymers (formerly Ausimont S.p.A.).

Synthesis of PUD and PU/PTFE composites

Polyurethane was synthesized following a prepolymer mixing process, by polyaddition of isophorone diisocyanate, poly(propylene glycol), 2-hydroxyethyl methacrylate, and dimethylol propionic acid (DMPA). The PU anionomer having 2-ethylmethacrylate terminal groups was dispersed in water containing chain extender (hydrazine) by prior neutralization of the carboxylic acid groups with triethylamine. The dispersion was degassed with nitrogen and then polymerized at 80 °C using potassium persulfate (0.15 wt% on HEMA base) as the initiator. The resulting polyurethane dispersion (PUD) was a stable dispersion with solid content of about 30 wt%. The particle size (by DLS measurements) was 114 nm, the zeta potential—56 mV, and the gel fraction value 94 %. More experimental details on the preparation of PUDs are given in a previous work (Pardini and Amalvy 2008).

The composites were prepared by mixing different amounts of PUD and nanoPTFE dispersion (from 2 to 50 wt%). The nanoPTFE dispersion was slowly

added, drop by drop, to the PUD, while continuously stirring for 5 min. The resulting products were stable dispersions with solid content of about 30 wt%. A shorthand notation is used in this paper to describe the blend systems. Thus, "90/10" denotes a system consisting of 90 wt% of PU and 10 wt% of nanoPTFE.

Film formation

Composite films were prepared by casting the dispersions on a Teflon® substrate and evaporating the water at 30 °C. Samples were then thermally treated (*cured*) at 60 °C for 48 h to allow complete coalescence.

Characterization

Fourier transform infrared spectra (FTIR)

Fourier transform infrared spectra (FTIR) of PU, nanoPTFE, and composite samples were obtained using a FTIR Nicolet 380 spectrophotometer, in transmission and ATR modes (64 scans and a resolution of 4 cm^{-1}).

X-ray photoelectron spectra (XPS)

XPS spectra were recorded using the SPECS Phoibos-150 high resolution hemispherical electron energy analyzer equipped with 9 channeltrons and one Al Kα1,2 X-ray source.

Contact angles and surface energies

Contact angle measurements have been carried out using a Model 500 goniometer (Ramé-Hart Instrument Co., USA) in the contact angle mode. Images were analyzed using the DROP image Advanced v2.2 software. All the tests were performed on the air-facing surfaces of the samples. Six measurements on different points were performed to calculate the mean static contact angle, θ. Among the different approaches enabling the determination of the different contributions to the surface energy of the solid based on contact angle measurements (Balkenende et al. 1998; Durrieu et al. 2004), we chose to work with the one proposed by Owens and Wendt (1969). Water, ethylene glycol, dimethyl sulfoxide, and 1-bromonaphthalene were used as probe liquids in terms of their polar and dispersive contribution.

Scanning and transmission electron microscopies

Scanning electron microscopy (SEM) images were obtained using a Jeol JSM-6460 (Japan) instrument. Samples were freeze-fractured using liquid nitrogen and sputtered with a Pd/Au blend before the observation. Transmission electron microscopy (TEM) studies were performed using a JEM 1200 EX II - JEOL instrument. Dilute dispersions were dried onto carbon-coated copper grids without metal coating.

Thermal properties

Melting temperatures of nanoPTFE and PU/nanoPTFE samples were determined by differential scanning calorimetry (DSC) using a Shimadzu DSC-60 instrument, running about 5 mg sample from room temperature to 340 °C, at a heating rate of 10 °C min^{-1}. A nitrogen gas purge was applied during analysis. Crystallization temperatures were determined on selected samples by applying heating and cooling cycles at ±10 °C/min from 200 °C up to 337 °C, just above the melting point of PTFE to avoid PU degradation.

Thermal gravimetric analysis (TGA) was obtained using a Shimadzu DTG-60 instrument, running also about 5 mg sample from room temperature to 550 °C at a heating rate of 10 °C min^{-1}.

Mechanical properties

Tensile properties (tensile strength, elongation at brake, and tension at brake) of the polymer films were measured at 25 °C using an EMIC DL-3000 tensile testing machine. Dog-bone-type specimens of 0.250 mm thickness, 6 mm width, and 33 mm length were prepared according to the test procedure given in ASTM D-638 (Type IV specimen), and a testing speed of 500 mm min^{-1} was used.

Roughness

The surface roughness analysis of the specimens was conducted using a Hommel Tester Basic T1000 machine and expressed in Ra values (Roughness average mm). The tracings were carried out five times, in five different locations, for each surface. The roughness was obtained by the arithmetic mean of these readings.

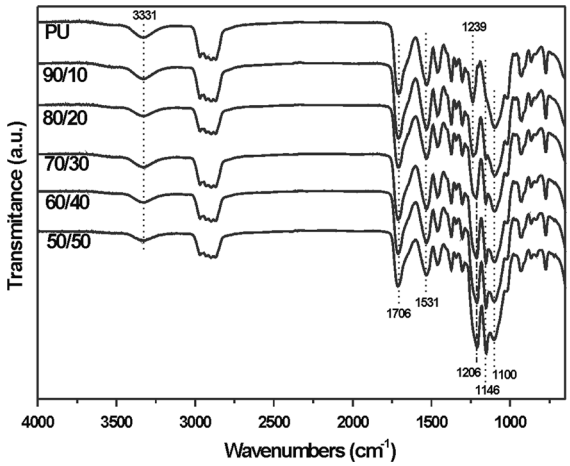

Fig. 1 ATR-FTIR spectra of PU and PU/nanoPTFE composites

Results and discussion

FTIR analysis

Figure 1 shows the FTIR spectra of PU and PU/nanoPTFE composites. The PU spectra demonstrates typical bands at around 3,331 cm^{-1} (N–H stretching vibrations), a broad band centered at 1,706 cm^{-1} (C=O stretching), a band at 1,531 cm^{-1} (Amide II band), a signal centered at 1,239 cm^{-1} (Amide IV band), and a band at 1,100 cm^{-1} (C–O-C stretching vibration of polyetherdiol) (Peruzzo et al. 2010).

A progressive change in the spectrum is observed in the composite samples, when increasing nanoPTFE content. Besides the bands of PU, characteristic PTFE peaks are observed (Yiang and Krimm 1956). The CF_2 stretching vibration of bulk PTFE occurs at the most intense IR absorption band, near 1,200 cm^{-1}. This band consists of two peaks at 1,207 and 1,152 cm^{-1} (not shown here) (Yiang and Krimm 1956). The CF_2 asymmetric stretching mode appears at 1,206 cm^{-1} as a shoulder of the Amide IV band in the 90/10 sample and it turns in a well-defined absorption band when its concentration increases. The intensity of the band located at 1,146 cm^{-1} assigned to the CF_2 symmetric stretching mode (Yiang and Krimm 1956) increases with the nanoPTFE content.

X-ray photoelectron spectra analysis

Figure 2 shows an example of the XPS analysis of the air-exposed surface samples. Figure 2a presents the

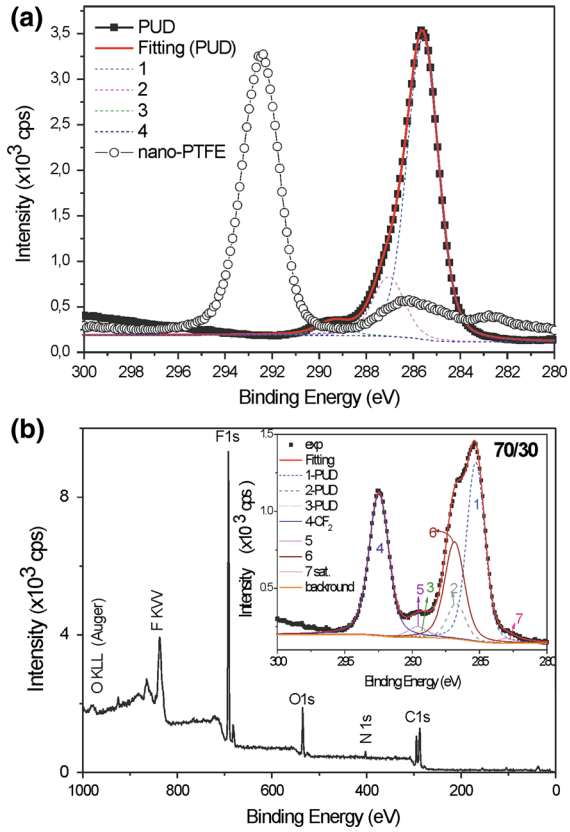

Fig. 2 **a** XPS spectra of C1s peak for pure PU and nanoPTFE. **b** Survey XPS spectra of B70:30 sample. *Inset* graph shows the C1s fitted components The peak label 7 is an X-ray satellite of component **4** (see text for details)

C1s peaks for pure PU as well as for the nanoPTFE sample and the PU fitting. Figure 2b displays the corresponding spectrum for the 30 wt% nanoPTFE sample. Table 1 shows the fragment concentrations at the surface for PUD, nanoPTFE, and PU/nanoPTFE samples.

As expected, peaks corresponding to carbon (C1s), nitrogen (N1s), oxygen (O1s), and fluorine (F1s) are detected. The inset shows the fitted components of the C1s peak where it is possible to identify contributions from both the PU (components **1**–**3**) and nanoPTFE. PU without nanoPTFE (Fig. 2a) was first fitted using three Lorentzian doublets (doublets were used due to the X-ray Al Kα1,2 character) with FWHM = 0.42 eV, each of them truly convoluted with a Gaussian function of FWHM = 1.29 eV, which takes into account the experimental broadening previously calibrated using Au 4f spectrum. Each of these

Table 1 Fragment concentrations at surface for PUD, nanoPTFE, and PU/nanoPTFE samples

Sample	Fragment concentration (%)								
	PUD	nanoPTFE	98/2	95/05	90/10	80/20	70/30	60/40	50/50
C1s-1(PU)	61.6	–	38.4	33.1	23.5	28.5	19.4	16.4	24.8
C1s-2(PU)	12.2	–	7.6	6.5	4.6	5.6	3.8	3.2	4.9
C1s-3(PU)	2.4	–	1.5	1.3	1.0	1.1	0.8	0.6	1.0
C1s-4(CF2)	–	35.1	3.8	7.3	14.9	9.9	17.5	17.8	16.5
C1s-5*	–	–	1.1	1.2	1.2	3.2	1.3	1.8	0.9
C1s-6**	–	–	13.9	15.6	10.9	13.1	12.0	13.6	10.6
O1s-1	10.8	37.3	2.5	7.4	14.7	10.6	15.8	16.9	14.5
O1s-2	9.4	27.7	4.6	7.8	15.1	12.8	14.3	15.6	14.7
N1s	3.5	–	11.9	10.1	7.0	6.3	6.1	6.6	7.1
F1s	–	–	14.7	9.7	7.1	8.9	8.9	7.4	5.0

* Component (**5**) is attributed to different hydrocarbon

** Component (**6**) is attributed to surface modifications of the nanoPTFE (see text)

components is related to carbamate group (C=O, C–O, C–N, and C–C). A contribution from the carboxylic group from DMPA moiety is also expected in peak 3 (Beamson and Briggs 1992).

To fit the complex spectra for PU/nanoPTFE systems, we have kept fixed the line widths, relative peak positions found for components **1**, **2** and **3** as well as the intensity ratio between them. In addition to those components, there are others clearly related to the nanoPTFE. Component **4** is observed, which can be assigned to the CF_2 groups (binding energy $\sim$292.5 eV), and is consistent with the bulk PTFE. Notwithstanding the concentration for such a component might be very sensitive to changes in F concentration(e.g., due possible effects of radiation damage typically observed in fluorinate polymers). There is also a clear component label 6 around 287 eV which also changes in intensity with the concentration of nanoparticles. This component is more difficult to be assigned, but could be associated with the ethereal carbon (C–O) contribution from the PPG soft segment due to an enrichment or orientation at the surface (Abdulkadir et al. 2006). A similar behavior was also observed in polyurethane-imide/clay hybrid coatings (Chattopadhyay et al. 2006). The incorporation of nanoPTFE clearly modifies the phase mixing of the segments of PU, as a consequence of additional hydrophobic interactions, and therefore the migration of the soft segments to the surface. However, the high resolution XPS of F 1 s (not shown here) indicates the presence of two components at 690.6 and 689.7 eV. Hydrogenated co-monomers like C_2H_4 and C_3H_6 are introduced during the last part of polymerization of PTFE dispersion to modify the surface properties (Marchese et al. 2001), so $–CH_2F_2–$ or $–C(CH_3)HF_2–$ species are formed. We found evidence of the former species in the FTIR spectra of a concentrated sample of nanoPTFE. Signals at 2,875 and 2,381 cm^{-1} for C–H stretching vibrations and at 720 cm^{-1} for rocking of $–CH_2–$ groups are observed among others. Therefore, the component **6** could be addressed to $–CH_2F_2–$ groups. The binding energy for $–CH_2–$ groups bonded to $–CF_2–$ is very close to the observed value for component **6**. For example, it is reported in the literature (Beamson and Briggs 1992) that for poly(vinylidene fluoride) $–(CF_2CH_2)_n–$ the binding energy is equal to 286.5 eV for C 1 s of the $–CH_2–$ group and 688.2 eV for the corresponding F 1s.

The atomic percentages of fluorine, both theoretically calculated (bulk composition) and measured values (surface composition) are given in Fig. 3. The relative concentration of Fluorine (F1s) and Carbon (C1s, component **4**) for CF_2 groups is consistent with bulk PTFE. Even though nanoparticles are present in the bulk, higher concentrations of particles appear at the surface for lower nanoPTFE contents. The result seems to be different to those found by comparing ATR and transmission FTIR spectra. However, the beam penetration in XPS assays is only around 5 nm, compared to 2 μm on the ATR experiments (ZnSe crystal, 45°).

Contact angle and surface energy

The wettability of the resulting films on PFTE substrates is evaluated by means of contact angle (CA) measurements.

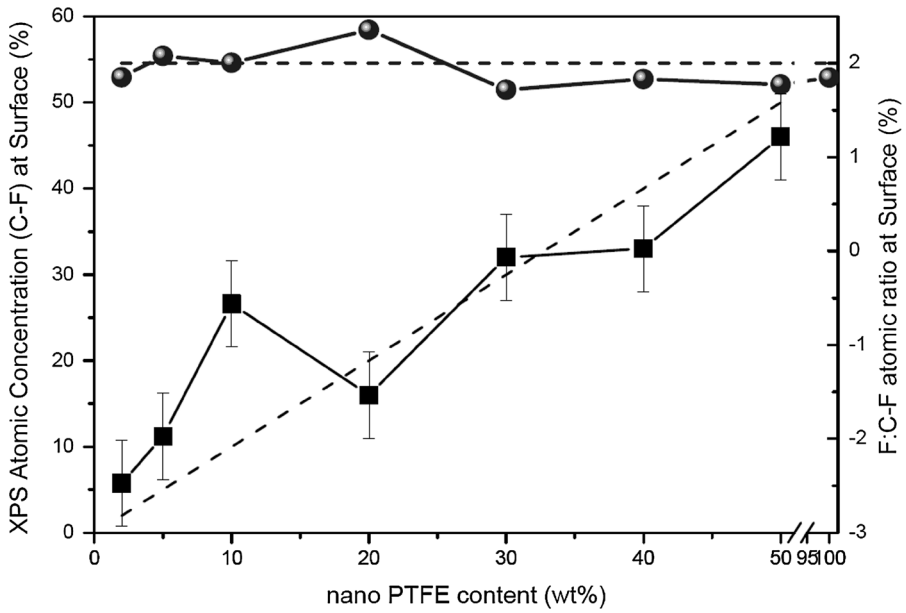

Fig. 3 Bulk and experimentally determined atomic compositions of the films

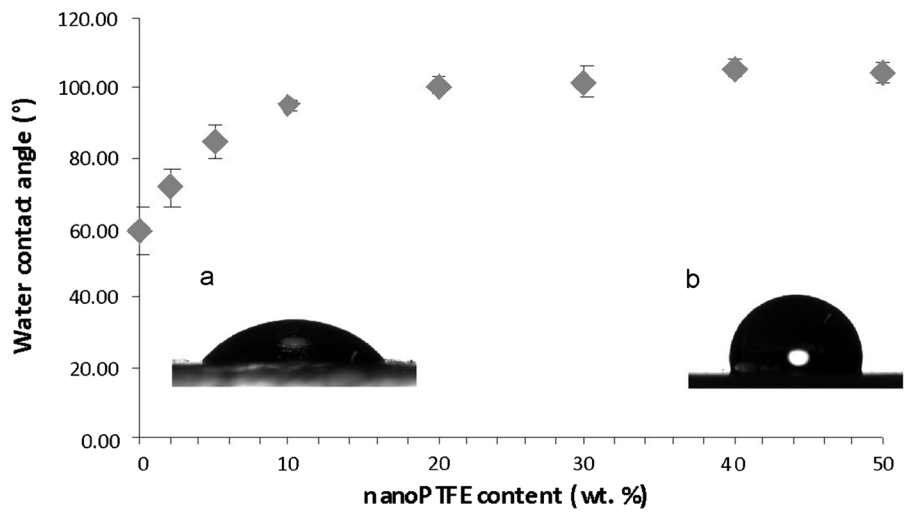

Fig. 4 Water contact angle variation with nanoPTFE content and typical water-drop images of PU (*a*) and PU/nanoPTFE 50/50 surfaces (*b*)

Figure 4 shows the water contact angle dependence on nanoPTFE particles content. The insets show typical water-drop images. It can be seen that the incorporation of 50 wt% of nanoPTFE changed the surface characteristics of the polyurethane film from hydrophilic (58.7°) to hydrophobic (104.3°).

The relationship between water CA and nanoPTFE content is not lineal and increases with increased nanoparticles content, when compared to pure polyurethane, reaching a maximum value for 20 wt% nanoPTFE (Fig. 4) indicating a more hydrophobic surface for this composition. The non-linear behavior could be explained by the accumulation of the nanoparticles to the air interface during the film formation (see XPS results). Beyond 20 wt%, the water CA remains almost constant probably due to saturation of the surface.

The total surface energy of these polymer films shows a marked decrease as nanoPTFE content increases. The polar contribution was higher in the

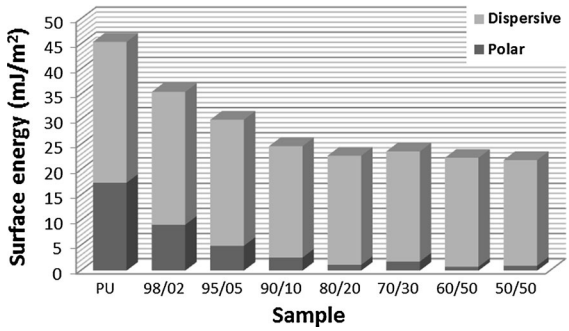

Fig. 5 Surface energies of PU/nanoPTFE composites

case of PU, because of the higher polarity of the urethane moiety. The Owens–Wendt method highlighted that this decrease came mainly from the polar contribution. This feature is clearly attributed to the PTFE nanoparticles which gave a corresponding decrease in the total surface energy values. All these features are clearly displayed in Fig. 5.

SEM and TEM

Figure 6 shows the SEM images of samples with 20, 30 y 50 wt% of nanoPTFE content.

SEM images showed important differences between PU and PU/nanoPTFE samples in the freeze-fracture surfaces. PU film presented a smooth and relatively featureless fracture surface morphology but, on the contrary, PU/nanoPTFE composites show a rough one. An attempt to incorporate additional nanoPTFE particles produced a much rougher pattern. It was attributed to the breakage of the matrix structure of the PU after adding nanoPTFE particles. The uniform rough pattern through the fracture surface suggests that the PTFE nanoparticles are present in the bulk.

Figure 6 shows also a typical TEM image of the samples prepared in this work (Fig. 6e). It can be observed that the particle size of the PU particles is about 170 ± 30 nm, which is higher than the particle size obtained by DLS probably due to a flattened of the soft material that compose the particles. On the other hand, nanoPTFE particles presented a particle size around 50 ± 10 nm, in agreement with the nominal average particle size indicated by the provider.

Thermal and mechanical properties

Differential scanning calorimetry

DSC analyses indicate that the melting temperature (T_m) of nanoPTFE changes by including them in the PU matrix. The melting of the nanoPTFE sample (Fig. 7a) occurs at 324.8 °C in agreement with the

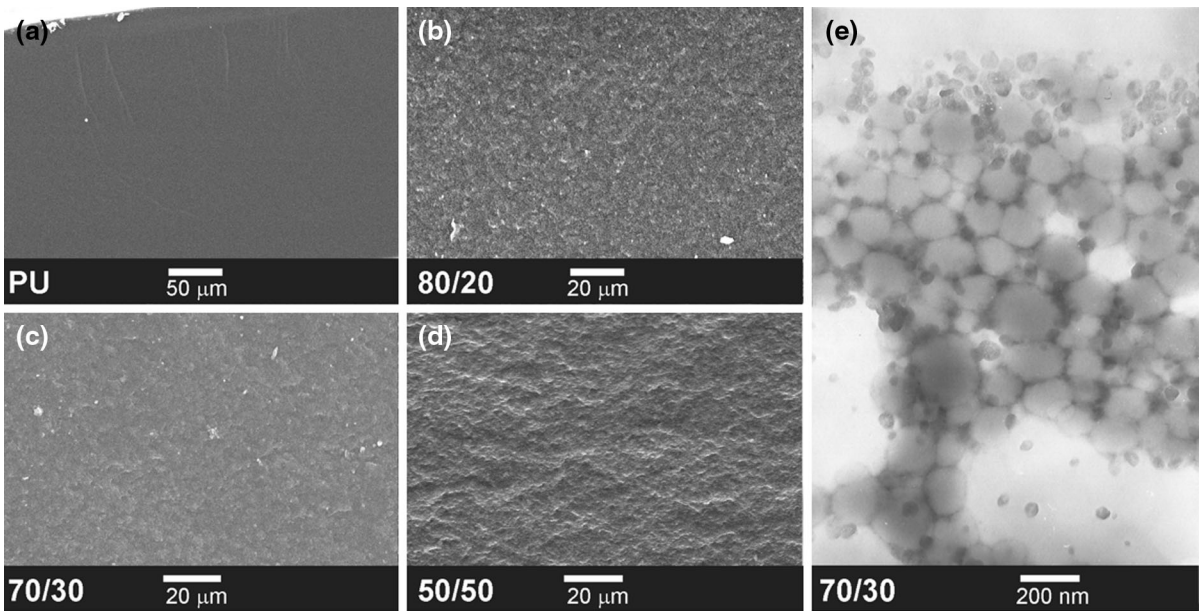

Fig. 6 SEM images for PU (*a*), 80/20 (*b*), 70/30 (*c*), 50/50 (*d*), and TEM image for 70/30 (*e*)

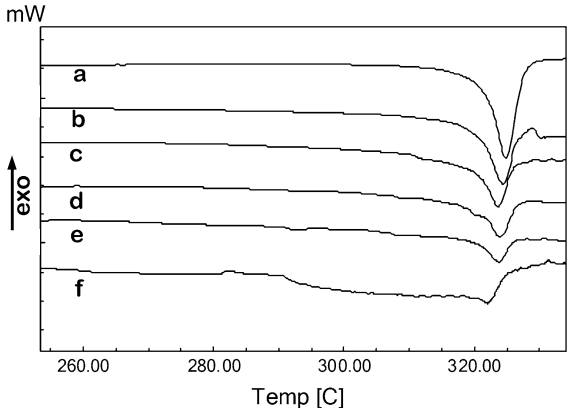

Fig. 7 DSC heating curves of nanoPTFE (*a*) and 50/50 (*b*), 60/40 (*c*), 70/30 (*d*), 80/20 (*e*), and 95/5 (*f*) PU/nanoPTFE composites

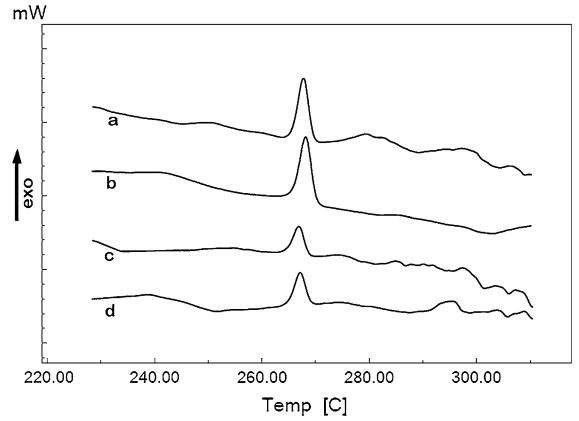

Fig. 8 DSC cooling curves for 95/5 (*a* 1st, *b* 2nd cycle) and for 98/2 (*c* 1st, *d* 2nd cycle) PU/nanoPTFE composites

literature data (Sparnacci et al. 2009). The T_m value for the nanoPTFE/PU 50/50 sample is observed almost at the same temperature. For the 60/40, 70/30, and 80/20 nanoPTFE/PU samples, a small shift of about 0.5 °C is observed (Fig. 7c, d, e) and for sample 95/5, the shift is 2.8 °C.

The shift of T_m to a slightly lower temperature could indicate some interaction between the PU matrix and the PTFE nanoparticles (Kapeliouchko et al. 2009).

It is well known that the melting point of nanoparticles is lower than the macroscopic material (Hosokawa et al. 2007). The lower melting point of PTFE observed in the PU/nanoPTFE indicates that nanoparticles are almost disaggregated.

To verify the dispersion degree of the PTFE nanoparticles at low concentrations, samples 95/5 and 98/2 were subjected to heating and cooling cycles at ±10 °C/min from 200 °C up to 337 °C (just above the melting point of the PTFE). Figure 8 shows the first and second cooling curves where the crystallization process is observed. For the 95/5 sample, the crystallization temperature is about 268 °C and for the 98/2 sample about 267 °C. Bulk PTFE crystallizes at 310 °C (Giani et al. 2003; Righetti et al. 2013a). The lower crystallization temperatures observed for 95/5 and 98/2 PU/nanoPTFE samples correspond to PTFE nanoparticles completely surrounded by the PU matrix (Giani et al. 2003; Pompe et al. 2005). A similar value of 270 °C was reported by Kapeliouchko et al. for PMMA/nanoPTFE core–shell particles (Kapeliouchko et al. 2009).

The second heating curves are very similar to the first ones, and no melting of bulk PTFE is observed at 310 °C, indicating no coalescence of nanoPTFE particles. These observations indicate that at nanoPTFE concentrations of 5 wt% or less the nanoparticles are very well dispersed in the PU matrix. Similar results were observed by Righetti et al. (2013b) in PTFE and polyethersulfone (PES) composites.

Thermal gravimetric analysis (TGA)

PTFE is stable up to 500 °C and TGA analysis indicates that by including nanoPTFE in the PU matrix, thermal resistance increases (Fig. 9). For example, the T_{10} stability temperature (temperature for 10 wt% decomposition) is 297 °C for PU and increases to 303 °C (90/10), 314 °C (80/20; 70/30), 318 °C (60/40), and 323 °C (50/50).

Mechanical properties

Table 2 shows the mechanical properties of studied systems, and they were affected by the incorporation of the PTFE nanoparticles. Low amounts of nanoPTFE improve tensile modulus, and the nanoPFTE particles are acting as a reinforcing material. The improvement in mechanical properties of films caused by the addition of hard particles to soft binder latex was also reported by Eckersley and Helmer (1997). However, both tensile strength and elongation at break are diminished when going to 20 wt% or higher content

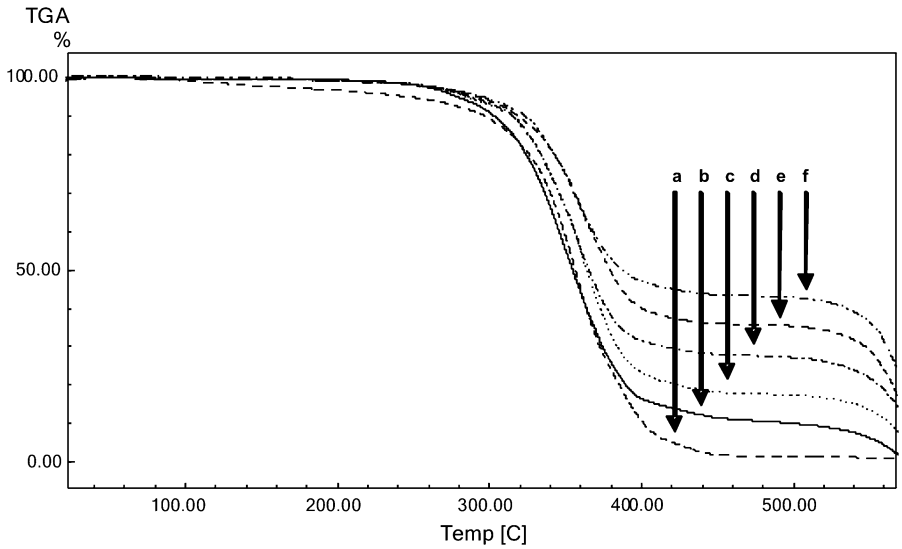

Fig. 9 TGA curves of PU (*a*) and PU/nanoPTFE composites: 90/10 (*b*), 80/20 (*c*), 70/30 (*d*), 60/40 (*e*), and 50/50 (*f*)

Table 2 Mechanical properties of PU and PU/nanoPTFE composites

	Tensile strength (MPa)	Elongation at break (%)	Tensile modulus (MPa)	Roughness (Ra) (mm)
PU	16.75 ± 0.75	236.2 ± 7.59	60.95 ± 6.22	0.13
90/10	17.81 ± 1.98	204.3 ± 23.53	107.90 ± 4.65	0.31
80/20	10.52 ± 0.66	161.3 ± 24.78	66.21 ± 3.84	0.32
70/30	6.62 ± 0.73	90.4 ± 13.49	56.30 ± 7.33	0.50
60/40	5.20 ± 0.42	90.3 ± 12.12	44.91 ± 2.96	0.31
50/50	–	–	–	0.13

indicating that the presence of particle aggregates induce fails, affecting the film elongation once the PU chains are oriented (since tensile modulus is not significantly affected). Righetti et al. (2013a) observed an increment in the storage modulus for 95/5 PES/PTFE composite and reduced values for 80/20 and 60/40 compositions.

On the other hand, roughness (Ra) increased for all concentrations up to 30 wt% and then decreased for higher concentrations. For 50 wt%, the Ra value is equal to that of the pure PU sample. This behavior is consistent with the idea that the nanoparticles accumulate in the film surface up to a concentration in which they agglomerate, stopping their migration to the surface.

Conclusions

Properties of PU films have been modified by the addition of PTFE nanoparticles and the contact angles of the composite films were higher than that of pure PU. XPS results indicate a higher concentration of nanoparticles at the film-air interface than in the rest of the sample, when nanoPTFE content is less than 10 wt%. Upon drying at room temperature, the soft PU particles ($T_g = 30$ °C) in the blend deform and pack to form a continuous matrix (phase separation) but the nanoPTFE particles retain their spherical shape ($T_g = 130$ °C). This phase separation is also favored by the negative surface charge of the particles ($\zeta_{PU} = -56$ mV; $\zeta_{nanoPTFE}$ −51 mV). In this way, the nanoPTFE particles separate and follow the drying front and self-stratified coating is then obtained. When polytetrafluoroethylene nanoparticles concentration increases, a percolation effect affects the phase separation process.

The thermal stability of the composite material increased, when increasing the nanoPTFE content. DSC analysis shows that for nanoPTFE particle concentrations less than 5 wt%, the nanoparticles are

well dispersed in the polymer matrix forming true polymeric nanocomposites. Also, the mechanical properties of low nanoPTFE content samples increased. The overall properties made these composite useful as low-energy surface coatings easily applied directly to the substrate by conventional methods. These nanoPTFE/PU dispersions could also be used as primers to improve the compatibility of PTFE with other materials.

Acknowledgments We thank CICPBA, ANPCyT (PICT 2011–0238), and CONICET for their financial assistance, L. F. Gambino and O.R. Pardini for technical assistance, Christopher Young for reviewing and correcting the paper and Solvay Specialty Polymers S.p.A. (Italy) for the donation of the nanoPTFE dispersion. PSA and PJP are the members of CONICET and JIA is the member of CICPBA (Argentina).

References

Abdulkadir A, Baki H, Yusuf M, Sefix S (2006) Synthesis, characterization and surface properties of amphiphilic polystyrene-b-polypropylene glycol block copolymers. Eur Polym J 42:740–750

Balkenende AR, van de Boogaard HJAP, Schloten M, Willard NP (1998) Evaluation of different approaches to assess the surface tension of low-energy solids by means of contact angle measurements. Langmuir 14:5907–5912

Beamson G, Briggs D (1992) High resolution XPS of organic polymers—the scienta ESCA300 database. John Wiley & Sons, New York

Chattopadhyay DK, Mishra AK, Sreedhar B, Raju KVSN (2006) Thermal and viscoelastic properties of polyurethane-imide/clay hybrid coatings. Polym Degrad Stab 91:1837–1849

Durrieu V, Gandini A, Belgacem MN, Blayo A, Eisele G, Putaux J-L (2004) Preparation of aqueous anionic poly-(urethane-urea) dispersions: influence of the nature and proportion of the urethane groups on the dispersion and polymer properties. J Appl Polym Sci 94:700–710

Eckesley ST, Helmer BJ (1997) Mechanistic considerations of particle size effects on film properties of hard/soft latex blends. J Coat Technol 69:97–107

Giani E, Sparnacci K, Laus M, Palamone G, Kapeliouchko V, Arcella V (2003) TFE − polystyrene core − shell nanospheres and nanocomposites. Macromolecules 36:4360–4367

Hosokawa M, Nogi K, Naito M, Yokoyama T (2007) Nanoparticle technology handbook. Elsevier, Amsterdam 18

Huang T, Lu R, Wang H, Ma Y, Tian J, Li T (2011) Investigation on the tribological properties of POM modified by nano-PTFE. J Macromol Sci B Phys 50:1235–1248

Jeong HY, Lee MH, Kim BK (2006) Surface modification of waterborne polyurethane. Colloids and surfaces A: physicochem. Eng Asp 290:178–185

Kapeliouchko V, Palamone G, Poggio T, Zuccheri G, Passeri R, Sparnacci K, Antonioli D, Deregibus S, Laus M (2009) PMMA-based core-shell nanoparticles with various PTFE cores. J Polym Sci A 47:2928–2937

Król P (2007) Synthesis methods, chemical structures and phase structures of linear polyurethanes. Prog Mat Sci 52:915–1015

Lai YK, Lin CJ, Wang H, Huang HY, Zhuang HF (2008) Superhydrophilic-superhydrophobic micropattern on TiO2 nanotube films by photocatalytic lithography. Electrochem Commun 10:387–391

Lakshmi RV, Basu BJ (2009) Fabrication of superhydrophobic sol–gel composite films using hydrophobically modified colloidal zinc hydroxide. J Colloid Interface Sci 339:454–460

Lee MH, Jang MK, Kim BK (2007) Surface modification of high heat resistant UV-cured polyurethane dispersions. Eur Polym J 43:4271–4278

Li M, Zhai J, Liu H, Song YL, Jiang L, Zhu DB (2003) Electrochemical deposition of conductive superhydrophobic zinc oxide thin films. J Phys Chem B 107:9954–9957

Liu H, Shang Q, Xiao G, Lv J (2011) Fabrication of stable superhydrophobic coatings with bicomponent polyurethane/polytetrafluoroethylene composites. Asian J Chem 23:2866–2870

Marchese E, Kapeliouchko V, Colaiana P (2001) TFE polymerization process. US Patent 6,297,334

Meng HF, Wang ST, Xi JM, Tang ZY, Jiang L (2008) Facile means of preparing super amphiphobic surfaces on common engineering metals. J Phys Chem C 112:11454–11458

Owens DK, Wendt RC (1969) Estimation of the surface free energy of polymers. J Appl Polym Sci 13:1741–1747

Pan LN, Dong HR, Bi PY (2009) Chemical preparation of aluminum superhydrophobic surface with nano-micro mixed structure by SDBS/HCl etching method. J Chin Univ-Chin 30:1371–1374

Pardini OR, Amalvy JI (2008) FTIR, ^{1}H-NMR spectra, and thermal characterization of water-based polyurethane/acrylic hybrids. J Appl Polym Sci 107:1207–1214

Peruzzo PJ, Anbinder PS, Pardini OR, Costa CA, Leite CA, Galembeck F, Amalvy JI (2010) Polyurethane/acrylate hybrids: effects of the acrylic content and thermal treatment on the polymer properties. J Appl Polym Sci 116:2694–2705

Pompe G, Häußler L, Adam G, Eichhorn K-J, Janke A, Hupfer B, Lehmann D (2005) Reactive polytetrafluoroethylene/polyamide 6 compounds. II. Study of the reactivity with respect to the functionality of the polytetrafluoroethylene component and analysis of the notched impact strength of the polytetrafluoroethylene/polyamide 6 compounds. J Appl Polym Sci 98:1317–1324

Righetti MC, Boggioni A, Laus M, Antonioli D, Sparnacci K, Boarino L (2013a) Thermal and mechanical properties of PES/PTFE composites and nano composites. J Appl Polym Sci 55:3624–3633

Righetti MC, Boggioni A, Laus M, Antonioli D, Sparnacci K, Enrico E, Boarino L (2013b) ageing reduction in PES through the incorporation of rigid non-interacting PTFE nano particles. Thermochim Acta 571:53–59

Sparnacci K, Antonioli D, Deregibus S, Laus M, Poggio T, Kapeliouchko V, Palamone G (2009) PTFE-based core-soft shell nanospheres and soft matrix nanocomposites. Macromolecules 42:3518–3524

Yamauchi G, Riko Y, Yasuno Y, Shimizu T, Funakoshi N (2005) Water-repellent coating for mobile phone microphones. Surf Coat Int B 88:281–283

Yiang CY, Krimm S (1956) Infrared spectra of high polymers. III. Polytetrafluoroethylene and polychlorotrifluoroethylene. J Chem Phys 25:563–571

Zheng ZR, Gu ZY, Huo RT, Ye YH (2009) Superhydrophobicity of polyvinylidene fluoride membrane fabricated by chemical vapor deposition from solution. Appl Surf Sci 255:7263–7267

Zhu MF, Zuo WW, Yu H, Yang W, Chen YM (2006) Superhydrophobic surface directly created by electrospinning based on hydrophilic material. J Mater Sci 41:3793–3797